Environmental Science & Technology

Article

pubs.acs.org/est

Controls on the Fate and Speciation of Np(V) During Iron (Oxyhydr)oxide Crystallization

Pieter Bots,[†] Samuel Shaw,[†] Gareth T.W. Law,[‡] Timothy A. Marshall,[†] J. Frederick W. Mosselmans,[§] and Katherine Morris*[,†]

[†]Research Centre for Radwaste Disposal and Williamson Research Centre for Molecular Environmental Science, School of Earth, Atmospheric and Environmental Sciences, The University of Manchester, Manchester, M13 9PL, United Kingdom

[‡]Centre for Radiochemistry Research and Research Centre for Radwaste Disposal, School of Chemistry, The University of Manchester, Manchester, M13 9PL, United Kingdom

[§]Diamond Light Source, Ltd., Diamond House, Harwell Science and Innovation Campus, Didcot, Oxfordshire OX11 0DE, United Kingdom

Supporting Information

ABSTRACT: The speciation and fate of neptunium as $Np(V)O_2^+$ during the crystallization of ferrihydrite to hematite and goethite was explored in a range of systems. Adsorption of NpO_2^+ to iron(III) (oxyhydr)oxide phases was reversible and, for ferrihydrite, occurred through the formation of mononuclear bidentate surface complexes. By contrast, chemical extractions and X-ray absorption spectroscopy (XAS) analyses showed the incorporation of Np(V) into the structure of hematite during its crystallization from ferrihydrite (pH 10.5). This occurred through direct replacement of octahedrally coordinated Fe(III) by Np(V) in neptunate-like coordination. Subsequent analyses on mixed goethite and hematite crystallization products (pH 9.5 and 11) showed that Np(V) was incorporated during crystallization. Conversely, there was limited evidence for Np(V) incorporation during goethite crystallization at the extreme pH of 13.3. This is likely due to the formation of a Np(V) hydroxide precipitate preventing incorporation into the goethite particles. Overall these data highlight the complex behavior of Np(V) during the crystallization of iron(III) (oxyhydr)oxides, and demonstrate clear evidence for neptunium incorporation into environmentally important mineral phases. This extends our knowledge of the range of geochemical conditions under which there is potential for long-term immobilization of radiotoxic Np in natural and engineered environments.

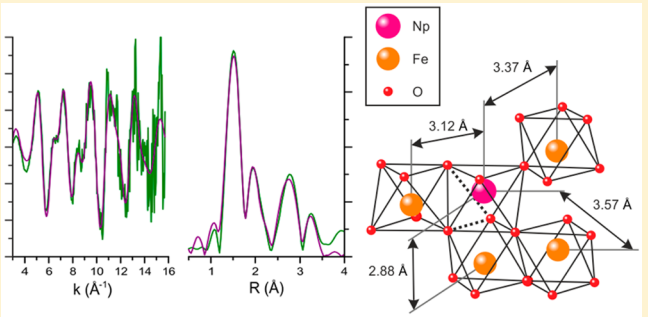

INTRODUCTION

Many nations have substantial nuclear legacy wastes due to their civil and military nuclear programs.[1−7] These materials contain significant levels of Np-237, an α-emitting radionuclide with a long half-life (2.14×10^6 y) which is highly radiotoxic and will be a significant dose contributing radionuclide in radioactive wastes on longer time scales.[5−8] Understanding the environmental behavior of Np is a key consideration at nuclear legacy sites such as Sellafield[4] and Hanford,[2,3] and for deep geological disposal of radioactive wastes.[5,6] In oxic environments, neptunium exists predominantly in the pentavalent oxidation state (Np(V) as neptunyl, NpO_2^+) with poorly soluble tetravalent neptunium (Np(IV) as Np^{4+}) dominant in more reducing environments.[1,5,6,9−13] Np(V) dominates in a wide range of oxic aqueous environments[5] and is expected to be the most soluble and mobile of the actinide species (solubility ~100 μM Np(V) at pH = 7).[5] Np(V) environmental mobility is controlled by a number of processes including its intrinsic solubility and sorption to minerals (e.g., iron (oxyhydr)oxide phases). Due to the reduced solubility of metal ions/radionuclides at elevated pH, base addition has been used to treat radioactive wastes,[14] and cementitious materials have been included in the engineering of geological disposal scenarios with the intention that this will increase pH and thus decrease the solubility and mobility of radionuclides.[15] For Np(V), the thermodynamic solubility decreases from ~100 μM at pH 7 to ~0.1 μM at pH 10.[5] With this in mind, we have focused on alkaline pH conditions (pH > 9) to allow specific insights into the fate of Np(V) during the transformation of ferrihydrite to crystalline iron (oxyhydr)oxide phases.

Iron(III) (oxyhydr)oxide phases such as ferrihydrite ($Fe_{9.74}O_{14}(OH)_2$),[16] hematite (Fe_2O_3)[17] and goethite (FeOOH)[18] are ubiquitous throughout the environment and

Received: November 12, 2015
Revised: February 19, 2016
Accepted: February 25, 2016
Published: February 25, 2016

DOI: 10.1021/acs.est.5b05571
Environ. Sci. Technol. 2016, 50, 3382−3390

will be present in nuclear decommissioning scenarios and radioactive waste materials.[19,20] Previous studies have shown that Np(V) strongly interacts with iron(III) (oxyhydr)oxide surfaces such as ferrihydrite,[21,22] lepidocrocite,[23] hematite[24−27] and goethite[28,29] with high distribution coefficients (K_D up to 10^5 mL/g).[30] These interactions typically occur through the formation of inner sphere Np(V) complexes[25] and, where carbonate is present, via Np(V)-carbonate surface complexes.[24] Additionally, the surface complexation behavior of Np(V) varies significantly with both pH[21,22,25−27] and carbonate concentration.[24,27] Despite its potential environmental significance, the mechanism(s) of Np(V) adsorption to ferrihydrite are not well understood, in particular spectroscopic information on Np(V)-ferrihydrite surface complexes is lacking. Additionally, there is a paucity of information on Np(V) incorporation into mineral structures despite the fact that this is potentially a highly effective mechanism to immobilize radionuclides. Interestingly, an early study suggested that Np(V) adsorbed to ferrihydrite may be incorporated during subsequent crystallization to hematite.[22] However, to date, no direct spectroscopic evidence exists for Np(V) incorporation into iron (oxyhydr)oxides in environmentally relevant systems. In comparison, spectroscopic studies have shown that both U(VI) and U(V) can substitute for Fe(III) in the structure of hematite.[31−33] This suggests, on the basis of the expected similarities in behavior of An(V, VI) species, that Np(V) may also undergo similar incorporation. Such sequestration processes have the potential to significantly limit the mobility of Np(V) in environmental systems. Furthermore, they could lead to irreversible binding of the radionuclide as long as the mineral-radionuclide assemblage is stable. Understanding the mechanisms of Np(V) incorporation and the factors controlling these processes will be essential in exploiting these reactions for remediating radionuclide contamination, and informing the long-term behavior of Np(V) in natural environments and nuclear decommissioning/radioactive waste management scenarios.

The aim of this study was to determine the potential for Np(V) incorporation into hematite and goethite during the crystallization of ferrihydrite under alkaline conditions. We induced the crystallization of ferrihydrite to hematite, goethite, or both in the presence of NpO_2^+ and under a range of experimental conditions at both trace and elevated Np(V) concentrations. Parallel inactive crystallization experiments were also performed and analyzed using X-ray diffraction (XRD) and transmission electron microscopy (TEM) to determine the effect of pH and temperature on the ferrihydrite crystallization pathway. A chemical extraction technique was used to explore the changes in Np(V) binding during iron (oxyhydr)oxide crystallization. Additionally, synchrotron based X-ray absorption spectroscopy (XAS) was used to directly determine the speciation of Np(V) throughout the crystallization reactions. This combined approach allowed us to distinguish between adsorption, precipitation and incorporation of Np(V) with the iron (oxyhydr)oxide crystallization products, and highlighted novel pathways by which Np(V) incorporates into the resultant mineral phases.

METHODS

Safety. Np-237 is a highly radiotoxic α-emitter with β- and γ-emitting daughter isotopes. Work with radionuclides must be carried out by appropriately qualified and experienced staff at facilities designed for work with radioactive materials. The possession and use of radioactive materials is subject to statutory control.

Experimental Design. The experiments were designed to bracket a range of elevated pH conditions where ferrihydrite was expected to crystallize to goethite, hematite and mixtures of these two minerals (Table SI1). Ferrihydrite was prepared according to the method of Cornell and Schwertmann.[33,34] For the nonactive crystallization experiments 0.2 mM $Ca(OH)_2$ was mixed with ferrihydrite at a solid solution ratio of 0.5 g l^{-1}. The pH was adjusted to either 9.5 or 11 using 10 M NaOH, and the crystallization reactions were induced at elevated temperature (80 °C) for up to 2 weeks. Two additional experiments designed to produce pure hematite or goethite were also performed. Hematite crystallization was induced in pH 10.5 NaOH with a 5 g l^{-1} ferrihydrite loading reacted at 120 °C for 4 weeks.[35−37] Goethite crystallization was induced in 0.1 M NaOH, 0.1 M KOH, and 0.3 mM $Ca(OH)_2$ at pH 13.3 with a 0.5 g l^{-1} ferrihydrite loading at room temperature for 2 weeks.[36,37] Throughout, experiments were run in a CO_2-free atmosphere. The crystallization products were analyzed using a Bruker D8 X-ray diffractometer (XRD); Rietveld analyses were performed on the XRD patterns using Topas 4−2.[38] Transmission electron microscopy images were taken on the final crystallization products using a Philips CM200 field emission gun TEM.

Neptunium Experiments. The ferrihydrite crystallization experiments to produce pure hematite and goethite, and the systems at pH 9.5 and 11 were repeated with 0.04−100 μM $Np(V)O_2^+$ (spiked with a 0.16 or 1.6 mM Np(V) stock solution)[1] under the same conditions as the nonactive experiments to yield parallel sets of both low and high Np(V) concentration experiments. The Np(V) stock solution was added to the experiment either at the start of the ferrihydrite crystallization, to assess incorporation processes during crystallization, or to the final crystallization products to assess adsorption processes (Table SI1). At the end of the experiments, aliquots of the experimental suspensions were filtered (<0.2 μm, nylon) to quantify the Np(V) concentration in solution. To assess the partitioning of Np(V) into the solids, a chemical extraction was performed by acidifying experiments with HCl to pH 2.5−3, which is below the adsorption edge of Np(V) on iron(III) (oxyhydr)oxides.[25,30,33] After 2 h, aliquots of the extracted suspensions were filtered (<0.2 μm nylon) and analyzed to determine the acid extractable Np(V) and to calculate the fraction of incorporated Np(V). All filtered solution samples were analyzed for total Np(V) using ICP-MS with Th-232 as an internal standard (Agilent 7500cx). Finally, the Np(V) containing solid phases from the experiments with elevated Np(V) (>2000 ppm of Np(V) associated with the solids) were sampled by centrifuging the experimental slurries and decanting the supernatant. The remaining solids were prepared as wet pastes for XAS analyses, mounted in approved XAS cells, and stored under an inert atmosphere at −80 °C prior to analysis.

X-ray absorption spectroscopy (XAS) on the Np L_{III}-edge were collected on the high Np(V) concentration samples from the pH 9.5 and 11 adsorption and crystallization experiments at the INE-Beamline at ANKA, Karlsruhe, Germany using a Ge(422) monochromator and 5-element Ge fluorescence detector (Table SI1).[39] XAS analyses on the high Np(V) concentration pure hematite and goethite samples were performed at B18 at Diamond Light Source, U.K., at the Np L_{III}-edge using a Si(111) monochromator and 9-element Ge

DOI: 10.1021/acs.est.5b05571
Environ. Sci. Technol. 2016, 50, 3382−3390

Table 1. Percentage of Np(V) Associated with the Solid/Crystalline Phases in Experimental Systems before and after Chemical Extraction

experiment	%Np in solid phase (pre-extraction)	%Np in solid phase (post-extraction)	quantitative XRD analysis[a]	crystallite size (XRD)
hematite	100(0)	94(2)	100% hematite	174.8 ± 3.3 nm
ferrihydrite adsorption pH 9.5	100(0)	7(2)	2-line ferrihydrite	no Bragg peaks[b]
hematite/goethite adsorption pH 9.5	100(0)	16(1)	17.3 ± 0.2% goethite;	46.7 ± 1.3 nm;
			82.7 ± 0.2% hematite[d]	70.2 ± 0.6 nm
hematite/goethite cryst. pH 9.5, 1 day	100(0)	72(0)	23.7 ± 0.4% goethite;	39.2 ± 1.3 nm;
			76.3 ± 0.4% hematite	57.7 ± 0.6 nm
hematite/goethite cryst. pH 9.5, 14 days	100(0)	90(1)	17.3 ± 0.2% goethite;	46.7 ± 1.3 nm;
			82.7 ± 0.2% hematite	70.2 ± 0.6 nm
ferrihydrite adsorption pH 11	100(0)	10(2)	2-line ferrihydrite	no Bragg peaks[b]
goethite/hematite adsorption pH 11	100(0)	6(2)	64.2 ± 0.3% goethite;	59.0 ± 0.7 nm;
			35.8 ± 0.3% hematite[d]	54.9 ± 0.8 nm[c]
goethite/hematite cryst. pH 11, 1 day	100(0)	79(1)	68.2 ± 0.3% goethite;	55.7 ± 0.7 nm
			31.8 ± 0.3% hematite	51.1 ± 1.0 nm
goethite/hematite cryst. pH 11, 14 days	96(0)	88(0)	64.2 ± 0.3% goethite;	59.0 ± 0.7 nm;
			35.8 ± 0.3% hematite	54.9 ± 0.8 nm
goethite	100(0)	22(3)	100% goethite	15.7 ± 0.1 nm

[a]The associated Rietveld analyses of the XRD patterns of reaction products were calculated as the percentage of crystalline phases (ferrihydrite, goethite and hematite) and the calculated crystallite size are also presented. Results from the Rietveld refinement on the XRD patterns shown in Figure SI1, the presence of ferrihydrite was identified from the characteristic broad peaks at ~30 and ~63°. [b]No Bragg peaks were present in the XRD patterns (Figure SI1) to calculate crystallite sizes. [c]The fraction of hematite and goethite in these samples is identical to the 14 days crystallization samples.

fluorescence detector (Table SI1).[40] During the XAS analyses, a zirconium foil was used both for energy calibration and as an in-line reference standard. XAS data reduction, analyses and fitting were performed using the Demeter software package.[41] Background subtraction and normalization were performed in Athena. Athena was also used for fitting the XANES data to identify energy positions of peaks. FEFF8[42] was used to calculate the Np scattering paths using the crystallographic information files (CIF) for $NaNpO_2(OH)_2{\cdot}H_2O$,[43] hematite (Fe_2O_3),[17] and goethite (α-FeOOH).[18] The Fourier Transform (FT in R-space) of the Np L_{III}-edge EXAFS spectra was fitted in Artemis. When fitting the EXAFS, the amplitude correction factor (S_0^2) was fixed at 1 throughout, and only the multiple scattering paths directly from the Np−O_{ax} bonds were included. The statistical validity of the addition of all scattering paths was evaluated using the F-test for EXAFS.[44]

RESULTS AND DISCUSSION

Iron (Oxyhdr)Oxide Crystallization and Np(V) Partitioning. The results from the XRD and TEM analyses are summarized in Table 1 and Figures SI1 and SI2. During the crystallization of ferrihydrite at pH 9.5 and 11 at 80 °C, a mixture of hematite and goethite formed. The goethite/hematite ratio in the crystallization products increased with increasing pH and decreased with crystallization time (Table 1) consistent with past work.[35−37,45] As intended, for the pure hematite and goethite experiments, the final crystallization products contained no trace of other mineral phases (Table 1 and Figures SI1 and SI2).[35−37] The mineral crystallite sizes calculated from XRD increased from 1 to 14 days of crystallization to ≥40 nm,[46,47] apart from the goethite formed at pH 13.3 which had significantly smaller crystallites (15.7 nm; Table 1).

Np(V) had a high affinity for the iron(III) (oxyhydr)oxide phases in all experiments with the vast majority of Np(V) (≥96%) sequestered from solution regardless of the experimental system (Table 1). The chemical extraction data showed significant differences in Np(V) desorption from the solids following crystallization (Table 1). For the adsorption samples, the majority of the Np(V) (84−94%) was released during the chemical extraction (Table 1) confirming that Np(V) was predominantly reversibly bound to the surfaces of the iron (oxyhydr)oxides. Conversely, only 6% of the Np(V) was released from the solid phase during the chemical extraction of the pure hematite sample (Table 1), indicating that the vast majority of the Np(V) was incorporated into hematite. During the chemical extraction of the crystallization products at pH 9.5 and 11 for 1 day (Table 1), 72 and 79%, respectively, of Np(V) remained associated with the solid product after the extraction. This fraction increased to 90 and 88%, respectively, after 14 days of crystallization at pH 9.5 and 11 (Table 1). The significant proportion of nonextractable Np(V) in these experiments suggested that incorporation processes dominated. Additionally, the increase in nonextractable Np(V) with time indicates that incorporation increased during aging similar to that observed for U(VI) incorporation into hematite.[33] In contrast, the chemical extraction on the pure goethite sample at pH 13.3 released 78% of the Np(V) into solution (Table 1) suggesting that Np(V) incorporation into the iron oxyhydroxide phase did not dominate at this very high pH.

Np XANES. Np L_{III}-edge XANES spectra were collected on selected samples prepared with the high Np(V) concentrations (>2000 ppm of Np) required for XAS analysis (Table SI1). The resultant XANES spectra, including NpO_2^+ and Np^{4+} standards[48−50] are plotted in Figure 1. In these spectra, two resonance features were identified between 17620−17627 eV and 17652−17657 eV (Figure 1, black arrows, and Table SI2). These resonance features result from multiple scattering from the actinide−axial oxygen (Np−O_{ax}) and the equatorial oxygen (Np−O_{eq}) scattering paths within the linear dioxygenyl actinyl ions, respectively.[51−55] The similarities between the Np(V) standards and the samples confirmed that Np(V) dominates in the reactions as expected. In the XANES of dioxygenyl actinide

DOI: 10.1021/acs.est.5b05571
Environ. Sci. Technol. 2016, 50, 3382−3390

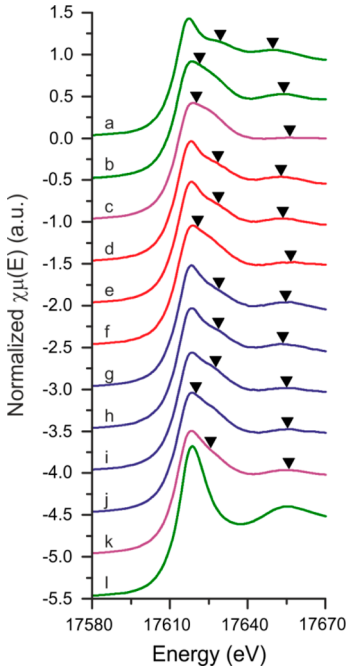

Figure 1. Np L_{III}-edge XANES spectra of the standards and samples: (a) aqueous neptunyl (NpO_2^+) standard,[48,49] (b) solid neptunate ($Na_3Np(V)O_4$) standard[50] (c) pure hematite, (d) ferrihydrite adsorption pH 9.5, (e) hematite/goethite adsorption pH 9.5, (f) hematite/goethite crystallization pH 9.5, 14 days, (g) ferrihydrite adsorption pH 11, (h) goethite/hematite adsorption pH 11, (i) goethite/hematite crystallization pH 11, 1 day, (j) goethite/hematite crystallization pH 11, 14 days, (k) pure goethite, and (l) aqueous Np^{4+} standard.[48,49] The arrows (▼) indicate the positions of the resonance features of the XANES fitted with Athena (Table SI2).

species, a shift in the energy position of the resonance features is inversely proportional to the axial and equatorial oxygen distances as observed for U(VI).[33,53,56] The positions of the two resonance features in the XANES spectra from the Np(V) adsorption samples match those of the Np(V) solution standard, indicating the Np(V) in these samples exhibit neptunyl-like coordination. In contrast, for the pure hematite sample, the first (17620.3 eV) and second (17656.0 eV) resonance features were clearly shifted to lower and higher energies, respectively, relative to the XANES from the aqueous neptunyl standard (Figure 1 and Table SI2). The XANES from the pure hematite sample is very similar to recent data from Na-neptunate (Na_3NpO_4; Figure 2 and Table SI2),[50] suggesting a change to a more neptunate-like Np(V) coordination environment during incorporation into hematite. In the XANES spectra from the crystallization samples at pH 9.5 and 11 and the pure goethite sample, the resonance feature positions appear intermediate between the Np adsorbed samples, and the neptunate-like pure hematite sample and Na-neptunate standard (Figure 1 and Table SI2). This reveals a change in the Np(V) local bonding environment during the crystallization of hematite, goethite, or both minerals.

Np(V) Adsorption to Iron(Oxyhydr)Oxides. The best fits to the EXAFS spectra from the adsorption samples indicate Np(V) is present within a 7-fold oxygen coordination environment with a neptunyl like configuration (Figure SI3 and Table 2) consistent with the XANES data. The modeled Np−O_{ax} bond lengths ranged from 1.83 to 1.85 Å with 5 equatorial oxygens at a distance of 2.38 to 2.42 Å, confirming essentially the same neptunyl-like coordination environment in all of the adsorbed samples. The equatorial oxygen bond lengths are marginally shorter than those observed for Np(V) adsorbed to hematite and goethite at pH 7−8.8 (between 2.46−2.51 Å).[24,25,28] This could be caused by positively charged neptunyl forming stronger and consequently shorter bonds with negatively charged hydroxide than with water at the increased pH values of the experiment, which is consistent with modeling studies of uranyl complexation with hydroxide and water.[57,58]

An additional Fe shell at 3.43 Å could also be fitted with statistical validity to the data from the ferrihydrite adsorption sample at pH 11 (Table 2). This is consistent with the adsorption of Np(V) via an inner sphere bidentate mononuclear surface complex at the ferrihydrite interface, and is in line with studies of Np(V) adsorption to other ferric (oxyhydr)oxide phases. In particular, Arai et al.[24] identified the formation of mononuclear bidentate complexes at the hematite surface with a similar Np−O coordination environment and an essentially identical Np−Fe bond length to that observed here. It was not possible to fit Np−Fe shells to the

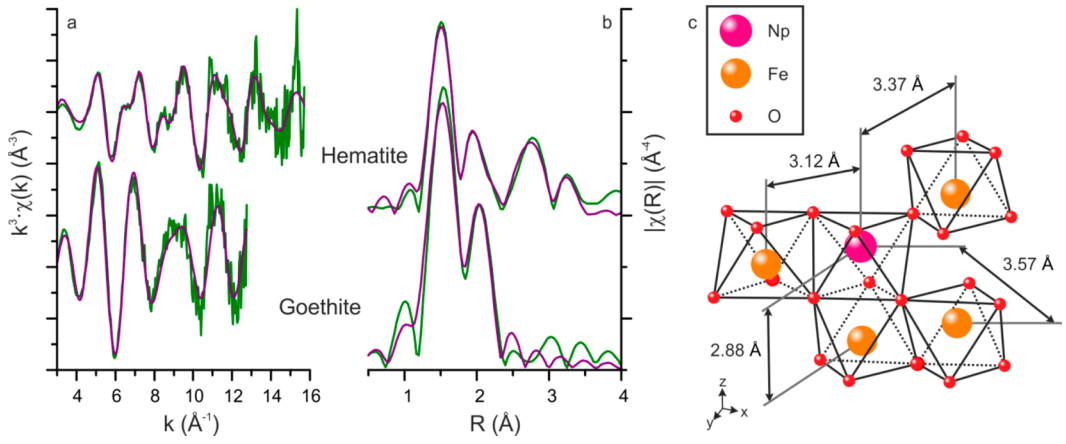

Figure 2. Np L_{III} (a) EXAFS spectra and (b) the corresponding FT of the EXAFS data from the pure hematite and goethite samples (green) and their respective best fits (purple). The FT are plotted without phase shift, and the fit parameters are detailed in Table 2. (c) Schematic representation of the coordination environment of Np(V) incorporated into the structure of hematite, including the Np−Fe distances based on the best fit (Table 2), based on the crystallographic information file for hematite.[17]

DOI: 10.1021/acs.est.5b05571
Environ. Sci. Technol. 2016, 50, 3382−3390

Table 2. Details of the Fits to the Np L_{III}-Edge EXAFS for Adsorption and Pure Hematite and Goethite Samples[a]

sample	path	CN[b]	R[b]	σ^2[b]	confidence (%)[c]
ferrihydrite adsorption pH 9.5	Np−O_{ax}	2	1.85(2)	0.004(2)	
R-factor = 0.0185[b]	Np−O_{eq}	5	2.42(4)	0.009(3)	92.1
ΔE_0 = 11.0(35)[b]					
fit range: k = 3−8.5; R = 1−3.5					
hematite/goethite ads. pH 9.5	Np−O_{ax}	2	1.85(2)	0.007(3)	
R-factor = 0.0222[b]	Np−O_{eq}	5	2.39(4)	0.008(2)	96.3
ΔE_0 = 8.5(33)[b]					
fit range: k = 3−8.5; R = 1−3.5					
ferrihydrite adsorption pH 11	Np−O_{ax}	2	1.83(1)	0.006(2)	
R-factor = 0.0094[b]	Np−O_{eq}	5	2.38(2)	0.007(2)	96.0
ΔE_0 = 8.4(17)[b]	Np−Fe	1	3.43(4)	0.004(2)	91.6
fit range: k = 3−8.5; R = 1−4	Np−O_{ax} MS	2	3.67	0.012	
goethite/hematite ads. pH 11	Np−O_{ax}	2	1.85(2)	0.008(3)	
R-factor = 0.0180[b]	Np−O_{eq}	5	2.39(3)	0.007(2)	96.1
ΔE_0 = 9.2(36)[b]					
fit range: k = 3−8.5; R = 1−3.5					
hematite	Np−O_{ax}	1	1.86(1)	0.0015(4)	
R-factor = 0.0084[b]	Np−O_{eq}	2	2.16(1)	0.006(1)	99.9
ΔE_0 = 3.6(16)[b]	Np−O_{eq}	3	2.38(1)	0.008(1)	100
fit range: k = 3−15; R = 1.2−3.5	Np−Fe	1	2.88(2)	0.011(1)	99.6
	Np−Fe	3	3.12(1)	0.011	99.9
	Np−Fe	3	3.37(2)	0.011	99.3
	Np−Fe	3	3.57(2)	0.011	99.3
	Np−O_{ax} MS	1	3.72	0.003	
goethite	Np−O_{ax}	2	1.88(1)	0.004(1)	
R-factor = 0.018[b]	Np−O_{eq}	2	2.23(2)	0.004(2)	98.8
ΔE_0 = 9.3(24)[b]	Np−O_{eq}	4	2.41(2)	0.004	92.0
fit range: k = 3−12.5; R = 1.3−3					

[a]The multiple scattering (MS) paths considered were the linear paths resulting from the Np−O_{ax} and the R and σ^2 parameters were evaluated as multiples of the corresponding single scattering path parameter. The amplitude correction factor ($S0^2$) in all fits was fixed at 1. [b]CN refers to the coordination number, R is the radial distance of the scattering path, σ^2 is the Debye−Waller factor, the *R*-factor is the goodness of fit parameter, ΔE_0 refers to the shift in energy from the calculated Fermi level, and the numbers in parentheses are the uncertainties calculated by Artemis (in the absence of uncertainties the coordination numbers were manually varied and fixed at the lowest R-factor and the σ^2 were linked to a previous scattering path). [c]Confidence refers to the statistical validity that the added scattering path improved the fit, calculated using the F-test for EXAFS.[44]

data from the remaining adsorption samples due to restricted data quality and/or, in the case of adsorption to the crystallization products at pH 9.5 and 11, the association of Np(V) with multiple surface sites offered by hematite and goethite (Table 1).

Np(V) Incorporation into Hematite. In the pure hematite sample, the chemical extraction showed that more than 90% of the Np(V) was incorporated into hematite particles. Modeling of the EXAFS spectra resulted in a best fit indicating a Np(V) species coordinated to 6 oxygen atoms with a range of Np−O distances from 1.86−2.39 Å (Figure 2 and Table 2). The Np(V) species could not be represented as a simple dioxygenyl species with two short Np−O_{ax} scattering paths. Rather, the best fit included a single short oxygen at 1.86 Å and two further oxygen shells at 2.16 and 2.38 Å. This suggests significant distortion in the overall Np−O local environment in pure hematite when compared to the neptunyl coordination environment of adsorbed and aqueous Np(V).[49] As EXAFS represents average coordination, it is possible that the fit represents an average of multiple Np−O local environments. The single oxygen at 1.86 Å could indicate that a fraction of the Np(V) has short axial oxygens in neptunyl coordination, with the remaining Np(V) having longer Np−O_{ax} bond lengths. Interestingly, the Np−O_{eq} coordination environment in the hematite sample (2 × 2.16 and 3 × 2.38 Å; Table 2) seems to closely match the Np−O coordination in sodium neptunate (2 × 2.09, 2 × 2.30, and 2 × 2.43 Å),[50] and the Np−O_{eq} bond lengths in the hematite sample are significantly shorter than those observed for the adsorbed, neptunyl species (2.38−2.42 Å, Table 2). Overall, the similarities of the Np−O coordination environment and the resonance feature positions in the XANES with sodium neptunate (Figure 1 and Table SI2)[50] confirm that Np(V) is incorporated into the structure of hematite in a distorted neptunate-like coordination environment. Such a coordination environment has also been observed for the incorporation of U(VI) within hematite.[31−33] However, the published U−O_{eq} bond distances when U is incorporated into hematite (2.07 and 2.23 Å)[33] are 0.09 and 0.15 Å shorter than the Np−O_{eq} bond distances we observe (2.16 and 2.38 Å, Table 2). This is despite the fact that the crystal radii of 6-fold coordinated U(VI) (0.87 Å) and Np(V) (0.89 Å) are almost identical.[59] Choppin et al.[60] report that the effective charge of U(VI) and Np(V) in uranyl and neptunyl species are +3.3 and +2.2, respectively. The reduced effective charge of Np(V) compared to U(VI) could account for the slightly elongated Np−O_{eq} bonds when compared to U−O_{eq} bond distances when structurally incorporated within hematite.

In addition to the neptunate-like oxygen scattering paths, iron scattering paths at four distances were included in the best fit of the EXAFS data from this sample. The Np−Fe bond

DOI: 10.1021/acs.est.5b05571
Environ. Sci. Technol. 2016, 50, 3382−3390

lengths (2.88, 3.12, 3.37, and 3.57 Å, with coordination numbers of: 1, 3, 3 and 3, respectively; Table 2) are within 5% of Fe−Fe distances in hematite (2.90, 2.97, 3.36, and 3.71 Å, Table SI3),[17] and similar to the U−Fe distances (2.87, 3.11, 3.45, and 4.01 Å)[33] when U is substituted for Fe(III) in hematite. The combination of the distorted Np−O coordination environment and the similarity of the Np−Fe to the Fe−Fe and U−Fe coordination environment in hematite confirms that Np(V) is directly substituting for octahedrally coordinated Fe(III) in the hematite structure (Figure 2c), via a similar mechanism to U(VI). The reduced coordination number of the most distant Fe shell, from 6 to 3 compared to the Fe and U(VI) coordination in hematite[17,33] (Table 2 and SI3), is too large to be caused by the creation of vacancies to compensate charge (see below). Rather, this reduced coordination may have resulted from the need to constrain the Debye−Waller factors for the Np−Fe scattering paths to the same value in the fitting for this sample (Table 2). Alternatively, the low coordination number may be due to higher concentration of Np(V) near to the surface of the hematite particles with a resultant reduction in the Fe coordination number of the outer Fe shell.

The direct substitution of Np(V) for Fe(III) will lead to an excess positive charge which must be compensated for e.g. via vacancy creation or changes in the Fe oxidation state.[61] To test for the creation of Fe(III) vacancies, we systemically decreased the coordination numbers of each Fe shell by 1. In every case, this resulted in a significant worsening of the fit. This suggests that if charge compensation occurs via the creation of Fe vacancies, that these are distributed randomly within the structure. In addition, there seems to be no clear mechanism to achieve charge compensation by reduction of Fe(III) in our fully oxidized system, therefore the exact mechanism of charge compensation remains elusive. Overall, the direct substitution of Np(V) for Fe(III) in the hematite structure highlights a novel pathway for Np(V) sequestration in natural and engineered systems where hematite forms which could significantly decrease the environmental mobility of this highly radiotoxic actinide.

Np(V) Partitioning during Mixed Hematite/Goethite Crystallization at pH 9.5 and 11. In the crystallization experiments at pH 9.5 and 11, chemical extraction data indicate > 79% of the Np(V) incorporated into the mineral following ferrihydrite crystallization to hematite and goethite (Table 1). In addition, the energy position of the resonance features in the XANES spectra became more like the pure hematite sample as increasing incorporation of Np(V) into the mineral assemblage occurred (Figure 1 and Table SI2). This suggests a systematic progression toward a more neptunate-like coordination environment. However, as the fraction of goethite increased in the crystallization samples (Table 1), the EXAFS spectra from these mixed crystallization experiments deviated from the EXAFS from the pure hematite sample (Figure SI4). Combined with the chemical extraction data highlighting increased incorporation into the crystallization products in these systems, this suggests that a fraction of Np(V) is incorporated into the structure of goethite. In addition, it indicates that the EXAFS includes contributions from Np(V) incorporated into both hematite and goethite. To explore the nature of the Np(V) interaction with goethite further, we extracted a residual EXAFS spectrum from the mixed crystallization samples by subtracting the adsorbed and pure hematite components from each EXAFS spectrum (Section SI1 and Figure SI5). Subsequent fitting of the resultant summed and normalized residual EXAFS resulted in a best fit with two Np−O_{ax} scattering paths at 1.87 ± 0.02 Å and 4 Np−O_{eq} scattering paths at 2.32 ± 0.03 Å (Table SI5). Interestingly, the Np−O_{eq} bond distances are in the range of Np−O_{eq} in hematite (Np−O_{eq} = 2.16 and 2.38 Å, Table 2) and shorter than those observed in the adsorbed Np(V) (Np−O_{eq} = 2.38−2.42 Å, Table 2). This shortening appears consistent with a more neptunate-like coordination environment confirming the observations from the XANES for these mixed systems. Overall, these data suggest that Np may also be incorporated into goethite at pH 9.5 and 11 with a neptunate-like coordination environment, although its precise location within the overall structure of goethite remains unresolved.

Np(V) Partitioning during Goethite Crystallization at pH 13.3. Increasing the pH of the crystallization from 11 to 13.3 resulted in a change in the partitioning of Np(V), with only 22% (Table 1) nonextractable Np(V) determined from the chemical extraction. In addition, the crystallization product transitioned to pure goethite with a significantly smaller crystallite size (15.7 nm; Table 1) than the goethite formed at lower pH (≥40 nm; Table 1). Subsequent EXAFS analyses of this sample (Figure 2 and Table 2), showed a best fit of Np(V) coordinated to 8 oxygens, with two axial oxygen backscatterers at 1.88 Å and two equatorial oxygen shells at 2.23 and 2.41 Å with coordination numbers of 2 and 4, respectively (Table 2). This Np(V) coordination environment is nearly identical to Np(V) in $NpO_2(OH)$, (Table 2 and Table SI3), suggesting that the Np(V) may be present as a discrete Np(V) hydroxide phase.[62,63] However, thermodynamic modeling for this system (PHREEQC, Table SI1)[64] showed undersaturation with respect to $NpO_2(OH)$ (SI: −0.42)[65] at 4 μM Np(V) and pH 13.3 (Table SI1), while the solution was predicted to be supersaturated with respect to $Ca_{0.5}NpO_2(OH)_2$ (SI: 3.37).[66,67] This suggests that a discrete Np phase which is soluble in the low pH chemical extraction may have formed although the exact phase is unknown. The precipitation of a U(VI) hydroxide has also been observed under similar high pH conditions ($NaUO_2O(OH)\cdot H_2O$)[56] and this prevented the incorporation of U(VI) into the structure of goethite.[68] This suggests that in these extreme pH systems, Np(V) (and more generally An(V,VI)) incorporation into the structure of goethite may be inhibited through the formation of discrete hydroxide precipitates. However, we cannot rule out the possibility that in this sample some of the Np(V) was adsorbed to goethite, and that the decreased crystal growth at pH 13.3 reduced the fraction of Np(V) incorporated due to limited overgrowth of the adsorbed Np. Overall, the lack of incorporation indicates Np(V) may remain labile under these high pH conditions with the aqueous concentration controlled by the Np(V)-phase solubility. Due to the discrepancy between the PHREEQC modeling and phase identity indicated by EXAFS, it is clear further work is required to determine Np(V) phase stability under high pH conditions and to generate accurate solubility data for these phases.

IMPLICATIONS FOR NEPTUMIUM BEHAVIOR IN THE ENVIRONMENT

Here, we define the fate of Np(V) during interactions with iron(III) (oxyhydr)oxide phases, including during crystallization of goethite and hematite, under a range conditions relevant to natural and engineered environments. Specifically, we show direct evidence for Np(V) adsorption to ferrihydrite via an inner sphere bidentate neptunyl surface complex. Following crystallization, this adsorbed Np(V) incorporates into hematite

DOI: 10.1021/acs.est.5b05571
Environ. Sci. Technol. 2016, 50, 3382−3390

via direct substitution for Fe(III) with a distorted neptunate-like coordination environment. This observed incorporation mechanism is broadly similar to U(VI) incorporation into hematite[31−33] and confirms that An(V, VI) can substitute for Fe(III) in the structure of hematite. This processes has the potential to immobilize Np(V) (and other An(V,VI) species) in systems where hematite is actively forming, potentially stabilizing the contaminants for extended timeframes, especially given the stability of hematite, which is found in geological settings older than 1 Ga.[69] With increasing pH (9.5 to 11) and at lower temperature, we also show that Np(V) can become incorporated into goethite, therefore extending the number of phases and the geochemical conditions under which the incorporation of Np(V) can occur. By contrast, under extremely high pH conditions (>13), which are relevant to cement systems,[15,56] Np(V) is not incorporated during iron (oxyhydr)oxide crystallization probably due to the precipitation of a discrete Np(V) hydroxide phase. Overall, we provide valuable new insights into Np(V)/iron oxide interactions which will open new pathways to remediate radionuclide contamination, and will inform prediction of the long-term behavior of the transuranic elements in natural and engineered environments.

■ ASSOCIATED CONTENT

Supporting Information

The Supporting Information is available free of charge on the ACS Publications website at DOI: 10.1021/acs.est.5b05571.

Text detailing the analyses of the EXAFS of the crystallization samples at pH 9.5 and 11; TEM images and XRD patterns of the final products from the pure hematite and goethite samples and crystallization samples at pH 9.5 and 11; EXAFS results and the corresponding fits, including the linear combination analyses of the crystallization analyses at pH 9.5 and 11; and tables detailing the experimental conditions, the positions of the multiple scattering resonance features, the structure of hematite and NpO_2OH, and the result from the fit to the normalized sum of the residuals of the EXAFS analyses from the crystallization samples at pH 9.5 and 11. (PDF)

■ AUTHOR INFORMATION

Corresponding Author

* E-mail: katherine.morris@manchester.ac.uk. Tel: +44 (0) 0161 275 7541.

Notes

The authors declare no competing financial interest.

■ ACKNOWLEDGMENTS

This project has been funded as part of the U.K. Natural Environment Research Council (NERC) BIGRAD consortium through Grant No. NE/H007768/1. Beamtime was funded by Grant SP9621 and SP10163 at Diamond Light Source. ANKA and INE are thanked for providing beamtime and laboratory access to support our beamtime runs and we also thank Dr. Kathy Dardenne and Dr. Jörg Rothe for assistance and for their insights and knowledge of working with Np samples. We also acknowledge funding from EnvRadNet which enabled us to perform the first UK XAS analysis of transuranic samples at the Diamond Light Source on beamline B18 and from EPSRC grant number EP/I036389/1. We also thank Dr. Steve Parry, Prof. Andy Dent and Richard Doull for radiological safety advice and assistance at Diamond. We thank Paul Lythgoe for his assistance with the ICP-MS analyses.

■ REFERENCES

(1) Law, G. T. W.; Geissler, A.; Lloyd, J. R.; Livens, F. R.; Boothman, C.; Begg, J. D. C.; Denecke, M. A.; Rothe, J.; Dardenne, K.; Burke, I. T.; Charnock, J. M.; Morris, K. Geomicrobiological redox cycling of the transuranic element neptunium. *Environ. Sci. Technol.* **2010**, *44* (23), 8924−8929.

(2) Maher, K.; Bargar, J. R.; Brown, G. E. Environmental speciation of actinides. *Inorg. Chem.* **2013**, *52* (7), 3510−3532.

(3) Felmy, A. R.; Cantrell, K. J.; Conradson, S. D. Plutonium contamination issues in Hanford soils and sediments: Discharges from the Z-Plant (PFP) complex. *Physics and Chemistry of the Earth, Parts A/B/C* **2010**, *35* (6−8), 292−297.

(4) Parry, S. A.; O'Brien, L.; Fellerman, A. S.; Eaves, C. J.; Milestone, N. B.; Bryan, N. D.; Livens, F. R. Plutonium behaviour in nuclear fuel storage pond effluents. *Energy Environ. Sci.* **2011**, *4* (4), 1457−1464.

(5) Kaszuba, J. P.; Runde, W. H. The aqueous geochemistry of neptunium: Dynamic control of soluble concentrations with applications to nuclear waste disposal. *Environ. Sci. Technol.* **1999**, *33* (24), 4427−4433.

(6) Dozol, M.; Hagemann, R. Radionuclide migration in groundwaters: Review of the behaviour of actinides (Technical Report). *Pure Appl. Chem.* **1993**, *65* (5), 1081−1102.

(7) *Geological Disposal Facilities for Radioactive Waste Specific Safety Guide*; International Atomic Energy Agency: Vienna, 2011.

(8) *Geological Disposal: Radionuclide behaviour status report*, NDA Report no. NDA/RWMD/043; Nuclear Decommissioning Authority: Cumbria, U.K., 2010.

(9) Newsome, L.; Morris, K.; Lloyd, J. R. The biogeochemistry and bioremediation of uranium and other priority radionuclides. *Chem. Geol.* **2014**, *363*, 164−184.

(10) Morris, K.; Butterworth, J. C.; Livens, F. R. Evidence for the remobilization of Sellafield waste radionuclides in an intertidal salt marsh, West Cumbria, U.K. *Estuarine, Coastal Shelf Sci.* **2000**, *51* (5), 613−625.

(11) Thorpe, C. L.; Morris, K.; Lloyd, J. R.; Denecke, M. A.; Law, K. A.; Dardenne, K.; Boothman, C.; Bots, P.; Law, G. T. W. Neptunium and manganese biocycling in nuclear legacy sediment systems. *Appl. Geochem.* **2015**, *63*, 303−309.

(12) Brookshaw, D. R.; Pattrick, R. A. D.; Bots, P.; Law, G. T. W.; Lloyd, J. R.; Mosselmans, J. F. W.; Vaughan, D. J.; Dardenne, K.; Morris, K. Redox interactions of Tc(VII), U(VI) and Np(V) with microbially reduced biotite and chlorite. *Environ. Sci. Technol.* **2015**, *49*, 13139−13148.

(13) Fröhlich, D. R.; Amayri, S.; Drebert, J.; Grolimund, D.; Huth, J.; Kaplan, U.; Krause, J.; Reich, T. Speciation of Np(V) uptake by Opalinus Clay using synchrotron microbeam techniques. *Anal. Bioanal. Chem.* **2012**, *404* (8), 2151−2162.

(14) Cantrell, K. J.; Um, W.; Williams, B. D.; Bowden, M. E.; Gartman, B.; Lukens, W. W.; Buck, E. C.; Mausolf, E. J. Chemical stabilization of Hanford tank residual waste. *J. Nucl. Mater.* **2014**, *446* (1−3), 246−256.

(15) Small, J. S.; Thompson, O. R., Modelling the spatial and temporal evolution of pH in the cementitious backfill of a geological disposal facility. In *Scientific Basis for Nuclear Waste Management XXXII*, Hyatt, N. C.; Pickett, D. A.; Rebak, R. B., Eds. **2009**; Vol. *1124*, pp 327−332.

(16) Michel, F. M.; Ehm, L.; Antao, S. M.; Lee, P. L.; Chupas, P. J.; Liu, G.; Strongin, D. R.; Schoonen, M. A. A.; Phillips, B. L.; Parise, J. B. The structure of ferrihydrite, a nanocrystalline material. *Science* **2007**, *316* (5832), 1726−1729.

(17) Blake, R. L.; Hessevick, R. E.; Zoltai, T.; Finger, L. W. Refinement of the hematite structure. *Am. Mineral.* **1966**, *51*, 123−129.

DOI: 10.1021/acs.est.5b05571
Environ. Sci. Technol. 2016, 50, 3382−3390

(18) Szytuła, A.; Burewicz, A.; Dimitrijević, Ž.; Kraśnicki, S.; Rżany, H.; Todorović, J.; Wanic, A.; Wolski, W. Neutron diffraction studies of α-FeOOH. *Phys. Status Solidi B* **1968**, *26* (2), 429−434.
(19) Hildred, K. L.; Townson, P. S.; Hutson, G. V.; Williams, R. A. Characterisation of particulates in the BNFL Enhanced Actinide Removal Plant. *Powder Technol.* **2000**, *108* (2−3), 164−172.
(20) Duro, L.; Domènech, C.; Grivé, M.; Roman-Ross, G.; Bruno, J.; Källström, K. Assessment of the evolution of the redox conditions in a low and intermediate level nuclear waste repository (SFR1, Sweden). *Appl. Geochem.* **2014**, *49*, 192−205.
(21) Girvin, D. C.; Ames, L. L.; Schwab, A. P.; McGarrah, J. E. Neptunium adsorption on synthetic amorphous iron oxyhydroxide. *J. Colloid Interface Sci.* **1991**, *141* (1), 67−78.
(22) Sakamoto, Y.; Ohnuki, T.; Senoo, M. Redistribution of neptunium(V) during the alteration of ferrihydrite. *Radiochim. Acta* **1994**, *66−67*, 285−289.
(23) Yang, C.; Powell, B. A.; Zhang, S.; Rao, L. Surface complexation modeling of neptunium(V) sorption to lepidocrocite (γ-FeOOH). *Radiochim. Acta* **2015**, *103* (10), 707−717.
(24) Arai, Y.; Moran, P. B.; Honeyman, B. D.; Davis, J. A. In situ spectroscopic evidence for neptunium(V)-carbonate inner-sphere and outer-sphere ternary surface complexes on hematite surfaces. *Environ. Sci. Technol.* **2007**, *41* (11), 3940−3944.
(25) Müller, K.; Gröschel, A.; Rossberg, A.; Bok, F.; Franzen, C.; Brendler, V.; Foerstendorf, H. In situ spectroscopic identification of neptunium(V) inner-sphere complexes on the hematite−water interface. *Environ. Sci. Technol.* **2015**, *49* (4), 2560−2567.
(26) Jain, A.; Rawat, N.; Kumar, S.; Tomar, B. S.; Manchanda, V. K.; Ramanathan, S. Effect of humic acid on sorption of neptunium on hematite colloids. *Radiochim. Acta* **2007**, *95* (9), 501−506.
(27) Kohler, M.; Honeyman, B. D.; Leckie, J. O. Neptunium(V) sorption on hematite (α-Fe_2O_3) in aqueous suspension: The effect of CO_2. *Radiochim. Acta* **1999**, *85* (1−2), 33−48.
(28) Combes, J. M.; Chisholm-Brause, C. J.; Brown, G. E.; Parks, G. A.; Conradson, S. D.; Eller, P. G.; Triay, I. R.; Hobart, D. E.; Miejer, A. EXAFS spectroscopic study of neptunium(V) sorption at the α-FeOOH/water interface. *Environ. Sci. Technol.* **1992**, *26* (2), 376−382.
(29) Tinnacher, R. M.; Zavarin, M.; Powell, B. A.; Kersting, A. B. Kinetics of neptunium(V) sorption and desorption on goethite: An experimental and modeling study. *Geochim. Cosmochim. Acta* **2011**, *75* (21), 6584−6599.
(30) Li, D.; Kaplan, D. I. Sorption coefficients and molecular mechanisms of Pu, U, Np, Am and Tc to Fe (hydr)oxides: A review. *J. Hazard. Mater.* **2012**, *243*, 1−18.
(31) Duff, M. C.; Coughlin, J. U.; Hunter, D. B. Uranium co-precipitation with iron oxide minerals. *Geochim. Cosmochim. Acta* **2002**, *66* (20), 3533−3547.
(32) Ilton, E. S.; Pacheco, J. S. L.; Bargar, J. R.; Shi, Z.; Liu, J.; Kovarik, L.; Engelhard, M. H.; Felmy, A. R. Reduction of U(VI) incorporated in the structure of hematite. *Environ. Sci. Technol.* **2012**, *46* (17), 9428−9436.
(33) Marshall, T. A.; Morris, K.; Law, G. T. W.; Livens, F. R.; Mosselmans, J. F. W.; Bots, P.; Shaw, S. Incorporation of uranium into hematite during crystallization from ferrihydrite. *Environ. Sci. Technol.* **2014**, *48* (7), 3724−3731.
(34) Cornell, R.; Schwertmann, U. *the Iron Oxides: Structures, Properties, Reactions, Occurrences and Uses*, 2nd ed.; Wiley-VCH: Weinham, 2003.
(35) Das, S.; Hendry, M. J.; Essilfie-Dughan, J. Transformation of two-line ferrihydrite to goethite and hematite as a function of pH and temperature. *Environ. Sci. Technol.* **2011**, *45* (1), 268−275.
(36) Shaw, S.; Pepper, S. E.; Bryan, N. D.; Livens, F. R. The kinetics and mechanisms of goethite and hematite crystallization under alkaline conditions, and in the presence of phosphate. *Am. Mineral.* **2005**, *90* (11−12), 1852−1860.
(37) Vu, H. P.; Shaw, S.; Brinza, L.; Benning, L. G. Crystallization of Hematite (α-Fe_2O_3) under alkaline conditions: The effects of Pb. *Cryst. Growth Des.* **2010**, *10* (4), 1544−1551.
(38) Bruker AXS, *TOPAS V4.2: General Profile and Structure Analysis Software for Powder Diffraction Data. User's Manual.* Bruker AXS: Karlsruhe, Germany, 2009, 2009.
(39) Rothe, J.; Butorin, S.; Dardenne, K.; Denecke, M. A.; Kienzler, B.; Loeble, M.; Metz, V.; Seibert, A.; Steppert, M.; Vitova, T.; Walther, C.; Geckeis, H. The INE-Beamline for actinide science at ANKA. *Rev. Sci. Instrum.* **2012**, *83*, 4.04310510.1063/1.3700813
(40) Dent, A. J.; Cibin, G.; Ramos, S.; Smith, A. D.; Scott, S. M.; Varandas, L.; Pearson, M. R.; Krumpa, N. A.; Jones, C. P.; Robbins, P. E. B18: A core XAS spectroscopy beamline for Diamond. *J. Phys.: Conf. Ser.* **2009**, *190*.01203910.1088/1742-6596/190/1/012039
(41) Ravel, B.; Newville, M. ATHENA, ARTEMIS, HEPHAESTUS: data analysis for X-ray absorption spectroscopy using IFEFFIT. *J. Synchrotron Radiat.* **2005**, *12*, 537−541.
(42) Ankudinov, A. L.; Ravel, B.; Rehr, J. J.; Conradson, S. D. Real-space multiple-scattering calculation and interpretation of x-ray-absorption near-edge structure. *Phys. Rev. B: Condens. Matter Mater. Phys.* **1998**, *58* (12), 7565−7576.
(43) Almond, P. M.; Skanthakumar, S.; Soderholm, L.; Burns, P. C. Cation - cation interactions and antiferromagnetism in Na[Np(V)-$O_2(OH)_2$]: Synthesis, structure, and magnetic properties. *Chem. Mater.* **2007**, *19* (2), 280−285.
(44) Downward, L.; Booth, C.; Lukens, W.; Bridges, F. A variation of the F-test for determining statistical relevance of particular parameters in EXAFS fits. *AIP Conf. Proc.* **2006**, *882*, 129−131.
(45) Davidson, L. E.; Shaw, S.; Benning, L. G. The kinetics and mechanisms of schwertmannite transformation to goethite and hematite under alkaline conditions. *Am. Mineral.* **2008**, *93* (8−9), 1326−1337.
(46) Burleson, D. J.; Penn, R. L. Two-step growth of goethite from ferrihydrite. *Langmuir* **2006**, *22* (1), 402−409.
(47) Jia, B.; Gao, L. Growth of well-defined cubic hematite single crystals: Oriented aggregation and Ostwald ripening. *Cryst. Growth Des.* **2008**, *8* (4), 1372−1376.
(48) Scheinost, A. C.; Schmeisser, N.; Banerjee, D.; Rossberg, A.; Denecke, M.; Dardenne, K.; Rothe, J.; Daehn, R. AcReDaS (formerly AcXAS). Actinide Reference X-ray Absorption Spectroscopy Database. https://www.hzdr.de/acxas 2013.
(49) Hennig, C.; Ikeda-Ohno, A.; Tsushima, S.; Scheinost, A. C. The sulfate coordination of Np(IV), Np(V), and Np(VI) in aqueous solution. *Inorg. Chem.* **2009**, *48* (12), 5350−5360.
(50) Smith, A. L.; Martin, P.; Prieur, D.; Scheinost, A. C.; Raison, P. E.; Cheetham, A. K.; Konings, R. J. M. Structural properties and charge distribution of the sodium uranium, neptunium, and plutonium ternary oxides: a combined X-ray diffraction and XANES study. *Inorg. Chem.* **2016**, *55*, 1569−1579.
(51) Farges, F.; Ponader, C. W.; Calas, G.; Brown, G. E., Jr Structural environments of incompatible elements in silicate glass/melt systems: II. U(IV), U(V), and U(VI). *Geochim. Cosmochim. Acta* **1992**, *56* (12), 4205−4220.
(52) Den Auwer, C.; Simoni, E.; Conradson, S.; Madic, C. Investigating actinyl oxo cations by X-ray absorption spectroscopy. *Eur. J. Inorg. Chem.* **2003**, *2003* (21), 3843−3859.
(53) Den Auwer, C.; Guillaumont, D.; Guilbaud, P.; Conradson, S. D.; Rehr, J. J.; Ankudinov, A.; Simoni, E. Theoretical chemical contribution to the simulation of the L_{III} X-ray absorption edges of uranyl, neptunyl and osmyl hydrates and hydroxides. *New J. Chem.* **2004**, *28* (8), 929−939.
(54) Denecke, M. A.; Dardenne, K.; Marquardt, C. M. Np(IV)/Np(V) valence determinations from Np L_3 edge XANES/EXAFS. *Talanta* **2005**, *65* (4), 1008−1014.
(55) Lozano, J. M.; Clark, D. L.; Conradson, S. D.; Den Auwer, C.; Fillaux, C.; Guilaumont, D.; Webster Keogh, D.; Mustre De Leon, J.; Palmer, P. D.; Simoni, E. Influence of the local atomic structure in the X-ray absorption near edge spectroscopy of neptunium oxo-ions. *Phys. Chem. Chem. Phys.* **2009**, *11* (44), 10396−10402.
(56) Bots, P.; Morris, K.; Hibberd, R.; Law, G. T. W.; Mosselmans, J. F. W.; Brown, A. P.; Doutch, J.; Smith, A. J.; Shaw, S. Formation of

DOI: 10.1021/acs.est.5b05571
Environ. Sci. Technol. 2016, 50, 3382−3390

stable uranium(VI) colloidal nanoparticles in conditions relevant to radioactive waste disposal. *Langmuir* **2014**, *30* (48), 14396−14405.
(57) Sherman, D. M.; Peacock, C. L.; Hubbard, C. G. Surface complexation of U(VI) on goethite (α-FeOOH). *Geochim. Cosmochim. Acta* **2008**, *72* (2), 298−310.
(58) Kaltsoyannis, N.; Hay, P. J.; Li, J.; Blaudeau, J.-P.; Bursten, B. E. Theoretical Studies of the Electronic Structure of Compounds of the Actinide Elements. In *The Chemistry of Actinide and Transactinide Elements*, 4 ed.; Morss, L. R.; Edelstein, N. M.; Fuger, J., Eds. Springer: Dordrecht, The Netherlands, 2010; Vol. *3*, pp 1893−2012.
(59) Shannon, R. D.; Prewitt, C. T. Effective ionic radii and crystal chemistry. *J. Inorg. Nucl. Chem.* **1970**, *32* (5), 1427−1441.
(60) Choppin, G. R.; Jensen, M. P. Actinides in Solution: Complexation and Kinetics. In *The Chemistry of Actinide and Transactinide Elements*, 4 ed.; Morss, L. R.; Edelstein, N. M.; Fuger, J., Eds. Springer: Dordrecht, The Netherlands, 2010; Vol. *4*. pp 2524−2621.
(61) Kerisit, S.; Felmy, A. R.; Ilton, E. S. Atomistic simulations of uranium incorporation into iron (hydr)oxides. *Environ. Sci. Technol.* **2011**, *45* (7), 2770−2776.
(62) Gaona, X.; Tits, J.; Dardenne, K.; Liu, X.; Rothe, J.; Denecke, M. A.; Wieland, E.; Altmaier, M. Spectroscopic investigations of Np(V/VI) redox speciation in hyperalkaline TMA-(OH, Cl) solutions. *Radiochim. Acta* **2012**, *100* (10), 759−770.
(63) Gaona, X.; Wieland, E.; Tits, J.; Scheinost, A. C.; Dähn, R. Np(V/VI) redox chemistry in cementitious systems: XAFS investigations on the speciation under anoxic and oxidizing conditions. *Appl. Geochem.* **2013**, *28*, 109−118.
(64) Parkhurst, D. L.; Appelo, C. A. J. *User's Guide to PHREEQC (version 2)—A Computer Program for Speciation, Batch-Reaction, One-Dimensional Transport, and Inverse Geochemical Calculations*. U.S. Geological Survey: Denver, CO, 1999.
(65) Guillaumont, R.; Fanghänel, T.; Neck, V.; Guger, J.; Palmer, D. A.; Grenthe, I.; Rand, M. H. *Update on the Chemical Thermodynamics of Uranium, Neptunium, Plutonium, Americium and Technetium*; Organisation for Economic Co-operation and Development, Nuclear Energy Agency: 2003.
(66) Altmaier, M.; Gaona, X.; Fanghänel, T. Recent advances in aqueous actinide chemistry and thermodynamics. *Chem. Rev.* **2013**, *113* (2), 901−943.
(67) Fellhauer, D.; Rothe, J.; Altmaier, M.; Neck, V.; Runke, J.; Wiss, T.; Fanghänel, T., Np(V) Solubility, Speciation and Solid Phase Formation in Alkaline $CaCl_2$ Solutions. Part I: Experimental Results. *Radiochim. Acta*, **2016**, 10.1515/ract-2015-2489.
(68) Gerth, J. Unit-cell dimensions of pure and trace metal-associated goethites. *Geochim. Cosmochim. Acta* **1990**, *54* (2), 363−371.
(69) Hitzman, M. W.; Oreskes, N.; Einaudi, M. T. Geological characteristics and tectonic setting of proterozoic iron oxide (Cu-U-Au-REE) deposits. *Precambrian Res.* **1992**, *58* (1−4), 241−287.

DOI: 10.1021/acs.est.5b05571
Environ. Sci. Technol. 2016, 50, 3382−3390